Wind and Structures, *Vol. 20, No. 2 (2015) 327-347*
DOI: http://dx.doi.org/10.12989/was.2015.20.2.327

Reynolds number effects on twin box girder long span bridge aerodynamics

Ramtin Kargarmoakhar, Arindam G. Chowdhury* and Peter A. Irwin

Department of Civil and Environmental Engineering and International Hurricane Research Center, Florida International University, Miami, FL, USA

(Received November 10, 2014, Revised January 1, 2015, Accepted January 5, 2015)

Abstract. This paper investigates the effects of Reynolds number (Re) on the aerodynamic characteristics of a twin-deck bridge. A 1:36 scale sectional model of a twin girder bridge was tested using the Wall of Wind (WOW) open jet wind tunnel facility at Florida International University (FIU). Static tests were performed on the model, instrumented with pressure taps and load cells, at high wind speeds with Re ranging from 1.3×10^6 to 6.1×10^6 based on the section width. Results show that the section was almost insensitive to Re when pitched to negative angles of attack. However, mean and fluctuating pressure distributions changed noticeably for zero and positive wind angles of attack while testing at different Re regimes. The pressure results suggested that with the Re increase, a larger separation bubble formed on the bottom surface of the upstream girder accompanied with a narrower wake region. As a result, drag coefficient decreased mildly and negative lift coefficient increased. Flow modification due to the Re increase also helped in distributing forces more equally between the two girders. The bare deck section was found to be prone to vortex shedding with limited dependence on the Re. Based on the observations, vortex mitigation devices attached to the bottom surface were effective in inhibiting vortex shedding, particularly at lower Re regime.

Keywords: Reynolds number effect; twin box girder bridge; vortex shedding; force and moment coefficient; pressure distribution; aerodynamic response

1. Introduction

In order to estimate wind loads for structural design of bridges and to predict the aerodynamic performance of the bridge cross section, usually wind tunnel tests are carried out on scaled models of the structure. To ensure the proper simulation of the aerodynamic/aeroelastic response of the structure in a wind tunnel, similitude of certain non-dimensional parameters is necessary. One such non-dimensional parameter, Reynolds number, represents the ratio of inertial force to viscous force in a fluid. Conventional small-scale tests are often performed at Re that is lower than its full-scale counterpart by a factor of about 10^2 to 10^3, thus violating the Re similitude by a large margin. This is largely for practical reasons since matching Reynolds number is not possible in conventional wind tunnels using small models and low wind speed. Testing at lower Re compared to the prototype is often considered to be representative of the aerodynamic loading and responses

*Corresponding author, Dr., E-mail: chowdhur@fiu.edu

http://www.techno-press.org/?journal=was&subpage=8 ISSN: 1226-6116 (Print), 1598-6225 (Online)

of the full-scale structure for sharp edged bluff bodies, such as buildings and bridges. This is due to the assumption that the separation point of the flow is fixed on a bridge or other bluff structures with sharp edges and they can have aerodynamic characteristics almost insensitive to Re as long as a Re of greater than 10,000 is reached (Larose and D'Auteuil 2006). However, several researches including some more recent literature (Barre and Barnaud 1993, Schewe and Larsen 1998, Larose *et al.* 2003, Larose and D'Auteuil 2006, Kazutoshi *et al.* 2007, Larsen *et al.* 2008, Asghari Mooneghi *et al.* 2014), show that wind loads and the response of bluff structures with sharp edges -- particularly bridges -- can be sensitive to Re effects. It was also shown that Re increase can reduce the imbalances of aerodynamic forces between the two girders for twin girder bridges (Lee *et al.* 2014).

The aerodynamic performance of any structure immersed in a fluid depends on different parameters, such as Re and turbulence characteristics, which can affect the flow separation and reattachment mechanism, laminar to turbulent boundary layer transition, and the behavior of shear layers and separation bubbles. It is known that Reynolds number can change the location of the laminar to turbulent transition point which subsequently modifies the structure of the wake (Schewe and Larsen 1998). Schewe (2001) tested three different bluff structures to explain the reason behind the Re sensitivity of the drag coefficient and Strouhal Number (St). It was noticed that with the Re increase, the location of laminar to turbulent transition point moved upstream and helped the flow to reattach to the section, leaving a smaller wake. Smaller drag force and smaller vortices, being shed at a higher frequency, resulted from the change in the location of transition point and a smaller wake region. It was concluded that different flow regimes can be distinguished based on the Re that could affect the St and magnitude of steady and unsteady forces (Schewe 2001). In order to minimize the Re effects on the aerodynamic behavior of bridges, Lee *et al.* (2014) successfully fixed the location of the separation point at the bottom of the deck by attaching a boundary layer trip strip to the bottom surface. This is similar to a movable pin that Schewe (2001) added to a circular cylinder section that reduced the Re dependency through stabilizing the location of the transition point.

One typical aeroelastic phenomenon which causes concerns in the design of modern multiple girder bridges is Vortex Induced Vibration (VIV) (Wu and Kareem 2012). VIV occurs when the frequency of the vortices shed from the body approaches the modal frequency of the bluff body, creating a resonance type motion in the structure. While VIV is mostly a limited amplitude vibration that does not lead to a failure directly, it can yield to fatigue damage in bridge members and discomfort for drivers. Larsen *et al.* (2008) performed free vibration testing on a model of the Stonecutters bridge, a twin girder bridge with mildly curved bottom plates, for a range of Re from 0.7×10^5 to 3.62×10^5, based on the individual girder width. While the velocity range and the amplitudes of vibration corresponding to the VIV were almost insensitive to the Re variation for the bare section, the modified section with the guide vanes showed significant Re sensitivity. In order to mitigate or more desirably to avoid vortex induced oscillations in bridges, evaluation of the Re effect can be important in so far as it can change both the Strouhal number (St) and the amplitude of vibrations during the lock-in phenomenon (Kubo *et al.* 1999, Larose and D'Auteuil 2006, Kazutoshi *et al.* 2007, Larose *et al.* 2012). The Re effect on flutter instability was investigated by Matsuda (2001) and it turned out that testing at higher Re inclined to increase the flutter wind speed for the given configurations.

The prototype Re for bridges often ranges between 10^6 and 10^7, especially for high wind events such as thunderstorms and tropical cyclones. Studies on Re effects pertaining to twin girder bridges, a type of design that is gaining popularity in recent years, are limited. In view of

the potential for Re effects on wind loads and wind-induced dynamic effects on twin box girder long span bridges, the current research was aimed at investigating the aerodynamics of such bridges under a range of Re as close as possible to its prototype counterpart. The key objective of this research was to investigate the effect of Re on the aerodynamic characteristics of twin girder bridges, including pressure distribution, wind induced forces, Strouhal number, and vortex shedding. In order to investigate the effects of Re on the bridge response, a 1:36 scale model of a two dimensional (2-D) section of a twin girder bridge, based on the section of the "East Span of the San Francisco-Oakland Bay Bridge" was constructed and tested using the Wall of Wind (WOW) open jet wind tunnel facility at Florida International University (FIU). High Reynolds numbers were reached by increasing the testing wind speed up to 48.2 m/s. Forces and pressures were measured using load cells and pressure taps to capture the static and fluctuating forces on the deck due to the approach flow. Vortex shedding sensitivity to the Re was evaluated for both the bare deck configuration and a section equipped with vortex generators. The efficacy of the vortex generators on mitigating vortex shedding was investigated for different Re regimes. The research findings can (1) help inform engineers designing double box girder bridges on the potential Re effects, and (2) provide guidance for laboratory Re similitude for twin box girder bridge sections. The present study is different from those documented in the literature in the following aspects:

- The cross section studied here was a double girder deck with trapezoidal cross section for each girder which has sharper edges and is bluffer compared to the more streamlined sections studied before.
- Vortex generators and guide vanes represent different approaches to vortex shedding mitigation. Previously, only the effects of guide vanes on vortex shedding were evaluated for different Re regimes. In this study, efficacy of vortex generators in mitigating vortex shedding has been evaluated for different Re regimes.

2. Experimental setup

2.1 Twin box girder bridge deck

In this study, the Re effects on the static force coefficients and fluctuating surface pressures for a twin box deck bridge were evaluated. To this end, the bare cross sectional shape of the eastern span of the San Francisco-Oakland bridge (East Bay Bridge) deck with the inclusion of the traffic barriers was selected and tested in a high Reynolds number regime ranging from 1.3×10^6 to 6.1×10^6. East span of the San Francisco-Oakland bay bridge is an asymmetric self-anchored suspension bridge with a main span of 385 m and back span of 185 m (Fig. 1). This bridge features a twin deck configuration carried by self-anchored suspension cables where the two decks are linked together with 10 m wide transverse beams every 20 m. The single deck chord length (C), total width (B) and height (H) of the bridge deck are 28 m, 71 m and 5.5 m, respectively (Fig. 1). Each girder resembles a trapezoidal cross section shape with aspect ratio close to the approach span of the Great Belt east bridge for which noticeable Re effects were observed (Schewe and Larsen 1998). The bike path that exists on the real bridge was not included in the test setup as it would have added to the complexity of maintaining model rigidity at high wind speeds. In the current study, Re effects on the efficacy of vortex generator devices for the mitigation of vortex shedding was also investigated. These devices are used for the real bridge and represent diverging

pairs of vertical rectangular plates attached to the bottom surfaces of both girders as shown in Fig. 1. As the name suggests, each pair of vortex generators are meant to facilitate the formation of a pair of counter rotating vortices which are supposed to promote reattachment of the flow to the bridge surface. The functionality of these vertical plates is to inject a strong high speed flow into the gap between the decks, thus inhibiting the periodic vortex shedding and mitigating vortex induced vibrations in the prototype bridge structure. The information on the bridge specifications was provided by T.Y. LIN INTERNATIONAL GROUP, which was involved in all phases of developing this bridge, from designing to construction.

2.2 Measurement instrument and test setup

For this study, a rigid pressure-tapped sectional model of the twin-deck bridge was tested using the 12-fan WOW at FIU. A length scale of 1:36 was used to simulate the aerodynamic geometry of the bridge deck. A sectional view of the bridge section model and the distribution of the pressure taps are shown in Fig. 2. The maximum span length of the model was 3 m. Two large streamlined end walls covered the two ends of the model to reduce the end effects and provide a 2-D simulation of the wind flow. The rigid model was made out of a wooden frame and was covered by Plexiglas plates to produce the cross-section shape. The model was equipped with five strips of pressure taps in order to measure fluctuating surface pressure distributions. One strip was located in the middle of the span and the other strips were located as shown in Fig. 3 to evaluate the span-wise distribution of pressures. Pressures were measured at a total of 280 points with a 512 channel Scanivalve Corporation pressure scanning system at sampling frequency of 512 Hz for a period of two minutes for each test case. Pressure scanners were placed at both ends of the model to reduce the pressure tube length. A transfer function designed for the tubing was used to correct for the tubing effects (Irwin *et al.* 1979).

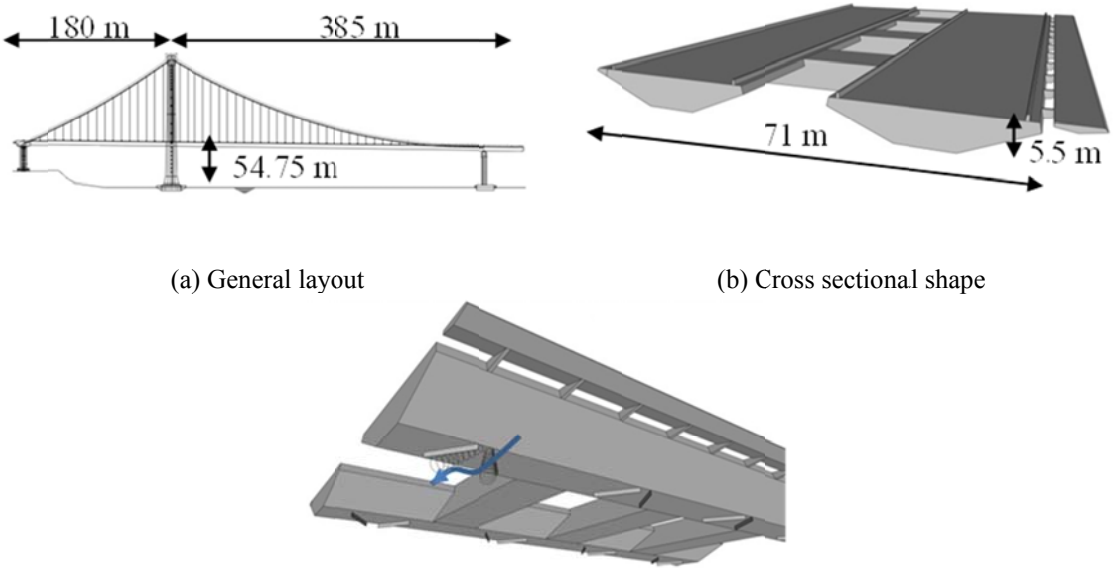

(a) General layout

(b) Cross sectional shape

(c) Vortex generators on the bottom surface

Fig. 1 East span of the San Francisco-Oakland bay bridge

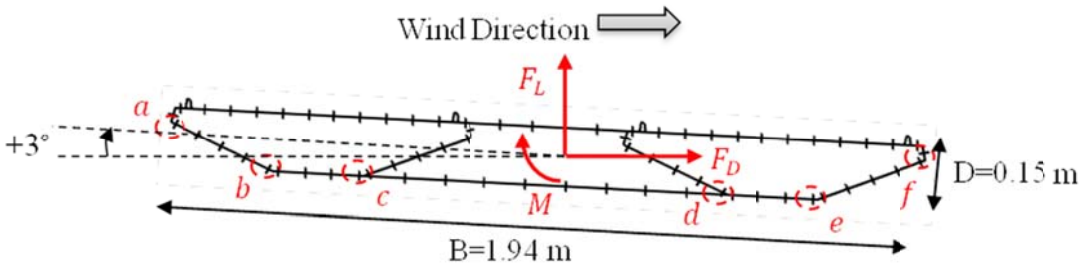

Fig. 2 Positions of the pressure taps (model is tilted to +3° angle of attack) a) Leading edge, b) Windward tipping edge of the upstream girder, c) Leeward tipping edge of the upstream girder, d) Windward tipping edge of the downstream girder, e) Leeward tipping edge of the downstream girder, f) Trailing edge

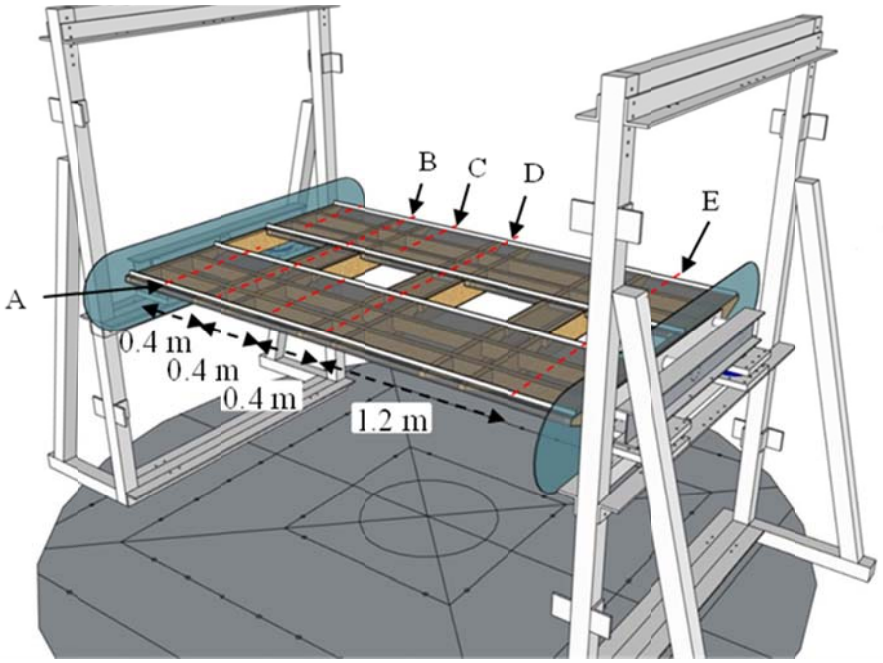

Fig. 3 Testing setup, "A" to "E" show the distribution of the chord-wise pressure tapped strips along the span length

Considering the width of the model to be equal to 1.94 m, the span to width ratio of the section model was 1.6. This ratio is similar to the ratio used in a previous research by Laima *et al.* (2013) to study the VIV of twin-girder bridges. Also, Piña and Caracoglia (2009) studied flutter derivatives for the Carquinez Strait Bridge using two models with different span to width ratios and suggested that span to width ratio of 1.7 was adequate for 2-D experiments.

The model for the current study was installed on an aluminum I-beam on each end using three aluminum pipe elements to allow for the simulation of various wind angles of attack by adjusting the pitch of the model (see Fig. 3). Five wind angles of attack were tested including -6°, -3°, 0°,+3°, and +6°. Positive angle was defined as the one which was measured from the horizontal to the axis of the bridge as shown in Fig. 2. Each beam was mounted on a pair of JR3 multi-axis load cells to measure the forces (Drag and Lift) and the pitching moment (see Fig. 3) simultaneously with the pressure measurements. All the data from force scanners were recorded using a CompactRIO data acquisition system at 100 Hz sampling rate. Both systems, load cells and pressure scanners, were used to facilitate comparison of wind effects.

2.3 Flow characteristics

The 12-fan WOW open jet facility at FIU was used to generate the wind field for the present study. WOW is capable of simulating Atmospheric Boundary Layer (ABL) mean wind speed profiles and turbulence characteristics. The nominal cross sectional dimensions of the testing section are 4.6 m × 6.1 m. Wind tunnel tests on bridges are often performed in flows with minimal turbulence as such flow produces conservative results. Gu *et al.* (2001) observed that flutter derivatives of the Jiangyin Bridge and a flat plate with aspect ratio of 22.5 were almost insensitive to the approaching flow turbulence. High turbulence can increase the diffusion of vortices and as a result reduce the vortex shedding strength (Wu and Kareem 2012). As a result, high turbulence has been found to be conducive for disrupting vortex induced vibration in bridges (Wardlaw *et al.* 1983). Thus, for the current study a flow condition with minimum turbulence was generated by removing the spires and floor roughness elements that are used in WOW for generation of ABL turbulence for testing building models. Fig. 4 shows a close-up view of the experimental apparatus in its final design, during the execution of the tests for the zero angle of attack.

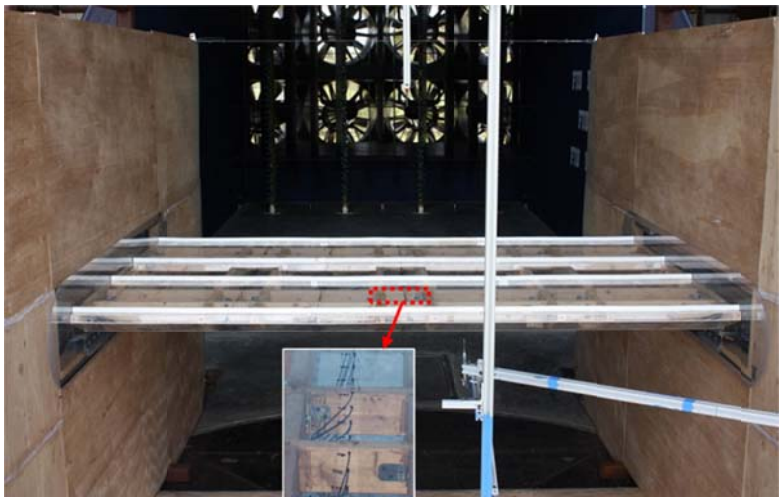

Fig. 4 1:36 scale model in front of Wall of Wind, Florida International University

Wind speeds were measured both during the tests on the bridge model and for free flow wind speed measurements (the bridge model was removed).

In order to measure the wind speeds during each test, two cobra probes were placed at 0.9 m below and above the middle point of the section to minimize the local effects of the model on the measured wind speed. The average of the measured wind speeds at these two points was used as the mean wind speed in the calculation of the pressure, force and moment coefficients.

For the free wind speed measurement, five cobra probes were used to measure the wind speeds (see Fig. 5). Two probes were installed at the same locations at which wind speeds were measured during the tests on models (probes 1 and 2). The other three cobra probes were installed at the bridge height, one at the center and the other two at equidistance between the center and the end walls (probes 3, 4, and 5). The ratio of the averaged wind speed of the two points at 0.9 m distant (probes 1 and 2) to the spatial average of measured wind speeds at the bridge height (average of probes 3, 4 and 5) was calculated for the free flow condition (i.e., $r = U_{avg\ \text{of probes 1 and2}} / U_{avg\ \text{of probes 3,4,and5}}$).The pressure, force and moment coefficients results were adjusted to the bridge height wind speed by multiplying each coefficient to r^2.

Data measured from the Cobra probes were collected at 100 Hz using the same CompactRIO data acquisition system that was used for force measurements. Tests were carried out for a range of wind speeds from 10 to 48.2 m/s, simulating Re values (based on the model width) between a range of 1.3×10^6 to 6.1×10^6. The Re for the prototype bridge can be estimated as 5.9×10^7 for wind speeds of 12.5 m/s, corresponding to the VIV lock-in wind speed for the first vertical mode of vibration at 0.214 Hz frequency. Based on the wind speed and turbulence measurements, the turbulence intensity and turbulence integral length scale were estimated as 3.0 percent and 0.2 m at the model height, respectively. Fig. 6 shows the non-dimensional power spectral density (PSD) of the longitudinal component of the turbulent wind speed, measured at the model height. In order to get a smooth representation of the spectra, averaging of the spectral analysis of 11 blocks was performed and presented here (each block was formed of 1024 points). Table 1 shows a summary of the tests carried out in this study.

Fig. 5 Cobra Probes Position

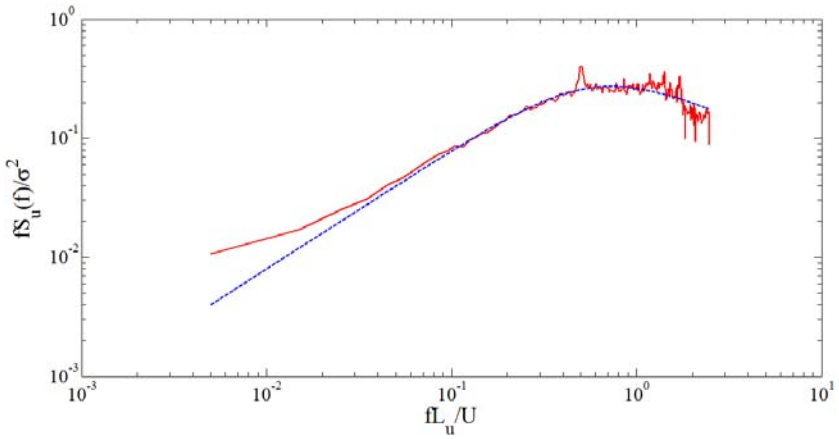

Fig. 6 Normalized power spectral density (PSD) of the longitudinal component of the wind speed at bridge height, ····· Karman Spectrum —— Simulated Spectrum

Table 1 Test Summary

Test case	Angle of attack	Wind speed (m/s)	Test duration (min)
Bare section	-6°, -3°, 0°, +3°, +6°	10.0-13.3-20.3-24-27.3-34.6-41.2-48.2	2
Section fitted with vortex generators	-6°, -3°, 0°, +3°, +6°	10.0-13.3-20.3-24-27.3-34.6-41.2-48.2	2

3. Parameters investigated for Re effects

At high Reynolds number, inertia forces dominate over the fluid viscous forces. At low Re, viscous forces have an increased effect on the aerodynamics. Re is dependent both to the model size and testing wind speed and is expressed as

$$Re = \frac{UB}{\nu} \tag{1}$$

where, U is mean wind speed (m/s), B is the reference dimension (in this case the deck width (m)), ν is kinematic viscosity of air (m^2/s).

For the case of constant kinematic viscosity, higher Re can be achieved only either by increasing the size of the model or the wind speed. The sensitivity of the following parameters to the Re was studied in the current work.

3.1 Pressure coefficients

Mean and fluctuating pressure distributions can be used to identify the regions of flow separation and reattachment in the studies of bluff body aerodynamics (Kwok *et al.* 2012). In this study, mean and fluctuating pressure distributions were considered in order to highlight the changes in the structure of the flow due to the Re variation. Pressure distributions are reported in

terms of non-dimensional mean and rms (root mean square) pressure coefficients ($C_{\bar{P}}$ and C_{σ_P}, respectively) obtained as

$$C_{\bar{P}} = \frac{P_{avg}}{1/2\rho U^2},\ C_{\sigma_P} = \frac{\sigma_P}{1/2\rho U^2} \tag{2}$$

where: P_{avg} is the mean pressure (N/m^2) obtained from the pressure time history data at each tap, σ_P is the standard deviation of pressure time history at each tap (N/m^2), ρ is the air density (kg/m^3), and U is the mean wind speed (m/s) at the model height.

3.2 Aerodynamic forces

Aerodynamic forces acting on the bridge deck can be expressed in terms of the two force components of Drag (F_D) and Lift (F_L) and the pitching Moment (M). As shown in Fig. 2, Drag is defined as the force component acting parallel to the wind direction, Lift is the force component perpendicular to the wind direction and pitching Moment is defined as the effective moment about the deck geometric center. C_D, C_L and C_M are the normalized form of the aerodynamic force/moment obtained, using the dynamic pressure and model dimensions, as

$$C_D = \frac{F_D}{\frac{1}{2}\rho U^2 LH}\ ,\ , C_L = \frac{F_L}{\frac{1}{2}\rho U^2 LB}$$

$$C_M = \frac{M}{\frac{1}{2}\rho U^2 LB^2} \tag{3}$$

where, F_D is the mean drag (N), F_L is the mean lift (N), M is the mean pitching (N·m), ρ is the air density (kg/m^3), U is the mean wind speed (m/s), and B, H and L represent the deck chord, deck height and the length of the model, respectively (m).

3.3 Self-excited forces

Self-exited forces induced by wind for a bridge deck, with vertical and torsional degrees of freedom (DOFs), are obtained from the following equations (Scanlan 1978)

$$L_h = \frac{1}{2}\rho U^2 B\left[KH_1{}^*(K)\frac{\dot{h}}{U} + KH_2{}^*(K)\frac{B\dot{\alpha}}{U} + K^2H_3{}^*(K)\alpha + K^2H_4{}^*\frac{h}{B}\right] \tag{4}$$

$$M_\alpha = \frac{1}{2}\rho U^2 B^2\left[KA_1{}^*(K)\frac{\dot{h}}{U} + KA_2{}^*(K)\frac{B\dot{\alpha}}{U} + K^2A_3{}^*(K)\alpha + K^2A_4{}^*\frac{h}{B}\right] \tag{5}$$

where, K is the reduced frequency ($2\pi fB/U$), f is the frequency of motion (Hz), h and α are the vertical and torsional displacements, over-dot indicates the derivatives with respect to time and $H_i{}^*$ and $A_i{}^*(i$ = 1 to 4) are flutter derivatives.

Memory effect causes aerodynamic forces to be influenced by structural motions. Therefore, it is hard to predict aerodynamic forces associated with structural motion from quasi steady theory. However, it has been shown that for high reduced velocities, quasi steady theory can predict aerodynamic forces associated with lateral and vertical motions satisfactorily (Chen and Kareem 2002). It has been also attempted to define derivatives corresponding to the torsional motion ($A_2{}^*$and $H_2{}^*$) from the quasi steady theory (Larose and Livesey 1997, Chen and Kareem 2002, Neuhaus and Höffer 2011). All of these studies related the $A_2{}^*$ parameter to $dC_M/d\alpha$.

However, an additional parameter was introduced in all cases which represented the

eccentricity between the point of application of the generated aeroelastic force and wind flow idealized point of incidence. It was shown that this parameter was not constant for different force components and different shapes (Chen and Kareem 2002, Neuhaus and Höffer 2011) which can cause error in the correct estimation of A_2^* and H_2^*. In addition, Schewe (2009) stated that the onset wind speed of torsional galloping is proportional to the inverse of $dC_M/d\alpha$.

The quasi-steady formulation for H_1^* is given by (Chowdhury and Sarkar 2004).

$$H_1^* = -\frac{1}{K}\left(\frac{dC_L}{d\alpha} + C_D\right) \tag{6}$$

where, $dC_L/d\alpha$ is the derivative of lift coefficient with respect to the angle of attack.

3.4 Vortex shedding

When wind blows over a bluff structure, flow separates and causes shedding of vortices periodically. This periodic vortex shedding exerts cross-wind forces on the body by creating fluctuating pressures. Strouhal number is a non-dimensional parameter that defines the dominant frequency of the fluctuations in the cross-wind force and is expressed as

$$St = \frac{fH}{U} \tag{7}$$

where, f is the frequency of vortex shedding (Hz), $H$is the bridge depth (m); U is the oncoming wind speed (m/s). *St* is a function of structure's geometry, turbulence intensity and Re. As stated earlier, vortex induced vibration VIV occurs when the frequency of vortex shedding approaches the natural frequency of the bluff body. The vortex shedding frequency can be obtained from the power spectral density (PSD) of the fluctuating lift force on the section. The peak evident in the fluctuating lift spectrum shows the frequency of the vortex shedding (Schewe and Larsen 1998, Kwok *et al.* 2012).

4. Experimental results and discussion

4.1 Re effects on stream-wise pressure distribution

Figs. 7- 9 show the distribution of mean pressures and rms of fluctuating pressures around the bare deck cross section. Negative mean pressures are shown outside of the bridge deck and positive mean pressures are shown inside of the bridge deck. Large (in magnitude) negative local pressures indicate the flow separation region. Fluctuating pressures represent the turbulent flow around the section which can be caused either by the intrinsic wind turbulence or the body induced turbulence (signature turbulence).

For the negative angles of attack, separation regions are noticed behind the traffic barrier on the top surface of both girders and at windward tipping edge at the lower surface of the upstream girder (see Figs. 7(a) and 7(b)). The fluctuating pressure distribution indicates that the downstream girder was immersed in the wake flow of the upstream girder (see Figs. 9(a) and 9(b)). This cross section was almost insensitive to the Re variation (for the Re interval tested here) when it was tilted to negative angles. This might be due to the fact that, traffic barriers fixed the location of the flow separation point on the top surface and therefore eliminated the Re sensitivity.

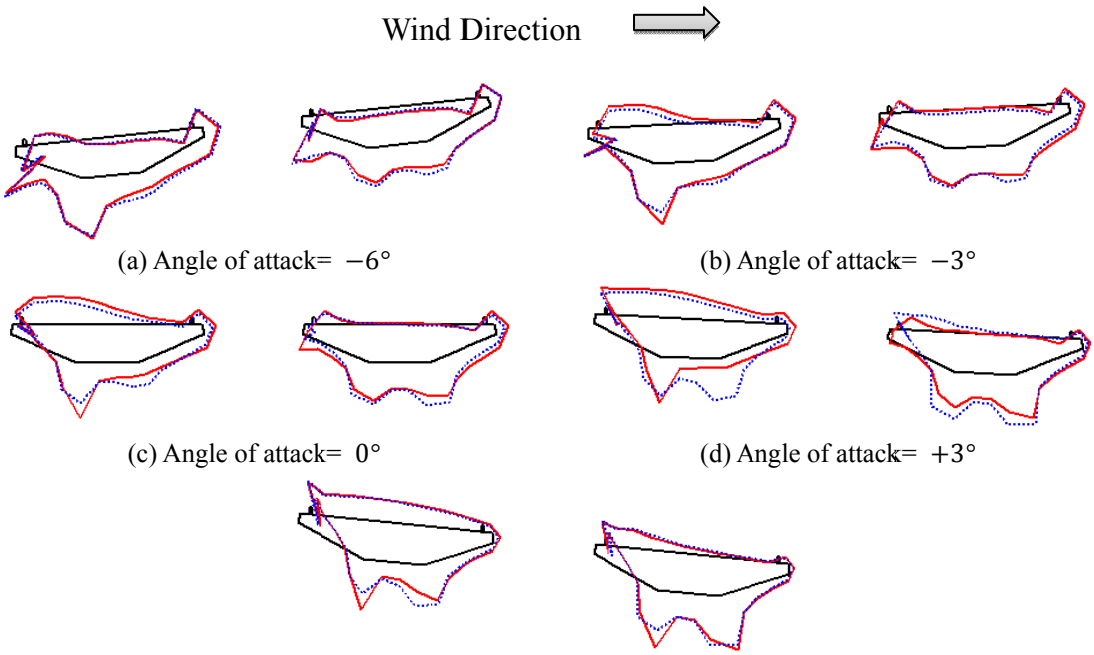

(a) Angle of attack= −6° (b) Angle of attack= −3°

(c) Angle of attack= 0° (d) Angle of attack= +3°

(e) Angle of attack= +6°

Fig. 7 Mean pressure distribution, 1.27×10^6 6.13×10^6.($C_{\bar{p}}$= 1: ⟷)

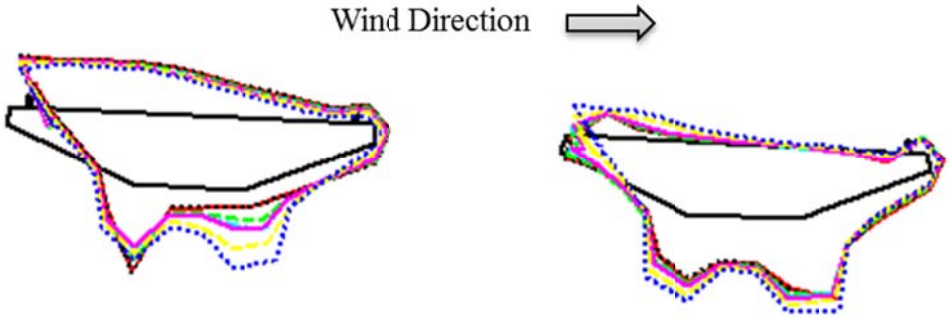

Fig. 8 Mean pressure distribution at +3° wind angle of attack, 1.27×10^6 1.70×10^6 2.60×10^6 3.47×10^6 4.40×10^6 5.24×10^6 6.13×10^6. ($C_{\bar{p}}$= 1:⟷)

For the zero wind angle of attack, Figs. 7(c) and 9(c) indicate flow separation at the traffic barrier location on the windward side of the upstream girder which created a turbulent flow across the top surface of both girders with no clear evidence of reattachment. The turbulence in the flow over the top surfaces is recognized from the appreciable magnitude of the rms of the fluctuating pressure (see Fig. 9(c)). Based on Fig. 7(c), for the lower ***Re*** regime, the flow was ventilated

through the gap in between the two girders due to the pressure difference between the top and bottom surfaces. Therefore the ventilation of flow through the gap created negative pressures on the windward inclined surface of the downstream girder. As the $\boldsymbol{Re}$ increased, the separated flow at the windward tipping edge of the upstream girder tended to reattach to the surface, creating a smaller wake in the downstream of the upstream girder and consequently a smaller drag on the upstream girder. Negative pressures on the windward inclined surface of the downstream girder were reduced with the $\boldsymbol{Re}$ increase, as the passing flow from the bottom of the upstream girder prevented the ventilation of the flow through the gap.

From Figs. 7(d) and 7(e), it can be concluded that the deck cross section was more sensitive to $\boldsymbol{Re}$ variation for the positive angles of attack. Flow over the top surface followed a similar trend to the case of zero angle of attack. This means that the flow was separated at the windward traffic barrier on the upstream deck and did not reattach to the surface while showing minimal sensitivity to $\boldsymbol{Re}$. However, as shown in Figs. 7(d) and 9(d), flow behavior changed with $\boldsymbol{Re}$ significantly on the lower side, particularly for the upstream deck. Separated flow at the windward tipping edge of the upstream girder reattached to the surface over a longer length but with a sharper slope for the higher $\boldsymbol{Re}$. This indicates that $\boldsymbol{Re}$ increase created a larger separation bubble on the bottom surface accompanied with a narrower wake region in the after body for the upstream girder, creating larger negative lift but smaller drag. Fig. 8 shows how the mean pressure distribution around the section at +3° wind angle of attack has changed gradually with the $\boldsymbol{Re}$ increase. Similar but less pronounced behavior was noticed for the +6° wind angle of attack (see Figs. 7(e) and 9(e)).

4.2 Re effects on force coefficients

Fig. 10 shows the variation of the mean drag, lift and moment coefficients due to the Re change for the bare section at zero wind angle of attack, measured with the load cells. From pressure distribution in Fig. 7(c), it can be concluded that with the Re increase, negative pressures on the downwind inclined surfaces of both girders decreased leading to a smaller drag. By increasing the Re, smaller separation zone formed on the top surface of the upstream girder that led to smaller negative pressures on this surface. With the Re increase, the negative lift coefficient increased in magnitude due to the modification of the pressure distribution around the two girders, particularly over the top and bottom surfaces (see Figs. 7(c) and 10(b)).

Fig. 11 shows the variation of the aerodynamic force coefficients**,** obtained from the load cells, with the angles of attack and Re for the bare section. Compared to the negative wind angles of attack, Re sensitivity was more pronounced for positive angles of attack, just as was indicated by the pressure distribution results (see Sec. 4.1). As discussed in Section 4.1, the windward traffic barrier on the top surface of the upstream deck dictated the location of the separation point, thus eliminating the Re sensitivity for the negative angles of attack. The drag coefficient showed a mild decreasing trend with the Re increase. The maximum decrease in drag coefficient due to Re variation was 24% for the positive 6 degree angle of attack. With the Re increase, flow separation became more prevalent at the leeward tipping edge of the upstream deck while flow reattachment on the leeward side of both girders led to a smaller wake. Smaller wake and accordingly lower negative pressure on the leeward inclined surface of the girders reduced the drag force. The magnitude of the changes due to Re in lift coefficients were on the order of 0.1. A larger separation at higher Re created a larger downward lift. The moment coefficient also showed some minor sensitivity to the Re variation.

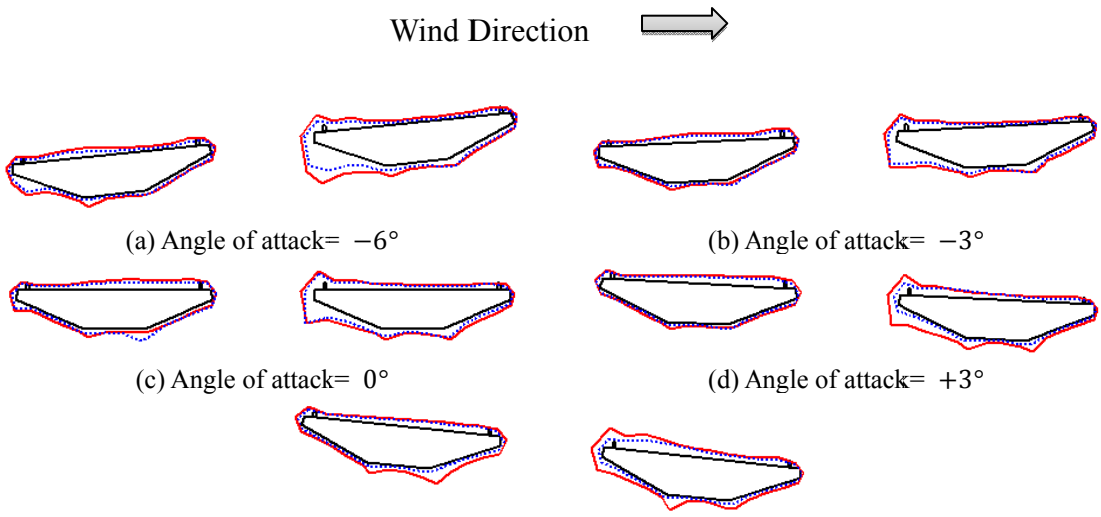

(a) Angle of attack= −6° (b) Angle of attack= −3°

(c) Angle of attack= 0° (d) Angle of attack= +3°

(e) Angle of attack= +6°

Fig. 9 rms of Fluctuating Pressure Distribution, 1.27×10^6 ····· 6.13×10^6. (C_{σ_p}= 0.5: ⟷)

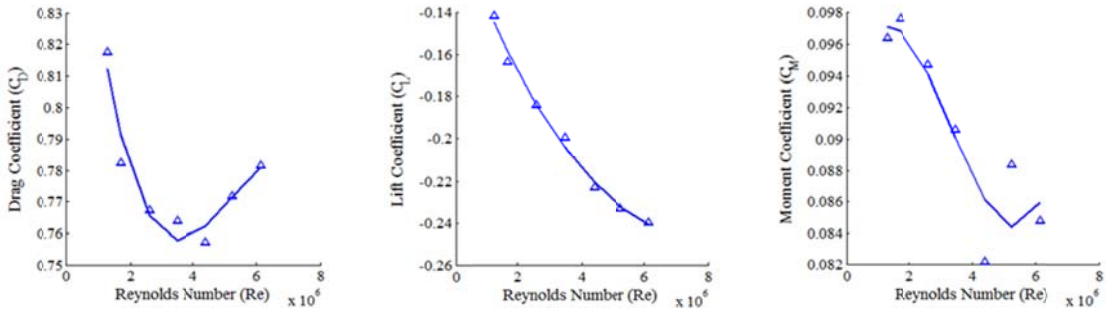

(a) Drag coefficient (b) Lift coefficient (c) Moment coefficient

Fig. 10 Force coefficients as a function of Reynolds number at 0° angle of attack, —△— Load Cells

Fig. 12 presents the derivative of force coefficients, obtained from load cells data, with respect to the angle of attack for the bare deck. Unlike $dC_D/d\alpha$ which showed little sensitivity to the Re variation, $dC_L/d\alpha$ and $dC_M/d\alpha$ were more Re sensitive, particularly for positive angles of attack. Based on quasi-steady theory, a negative value of $dC_L/d\alpha$ results in a positive value for ${H_1}^*$ that shows a potential for vertical galloping. As shown in Fig. 12, negative ${H_1}^*$ only happened for positive angles of attack (mainly for +6°). Increasing the Re changed the sign for $dC_L/d\alpha$ from negative to positive. This means that while testing at lower Re regime can show aerodynamic instabilities, the section was more aerodynamically stable at higher Re regimes. Kazutoshi *et al.* (2007) also addressed that testing for flutter stability in a low Re regime is conservative.

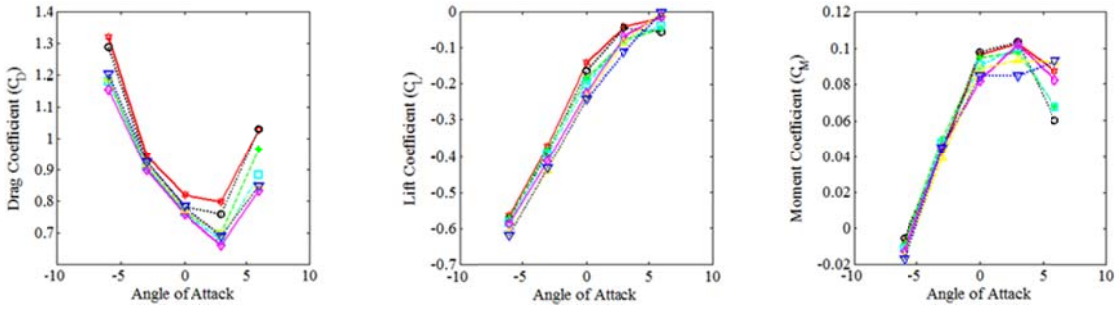

(a) Drag coefficient (b) Lift coefficient (c) Moment coefficient

Fig. 11 Static aerodynamic coefficients as a function of wind angle of attack, 1.27×10^6 1.70×10^6 2.60×10^6 3.47×10^6 4.40×10^6 5.24×10^6 6.13×10^6

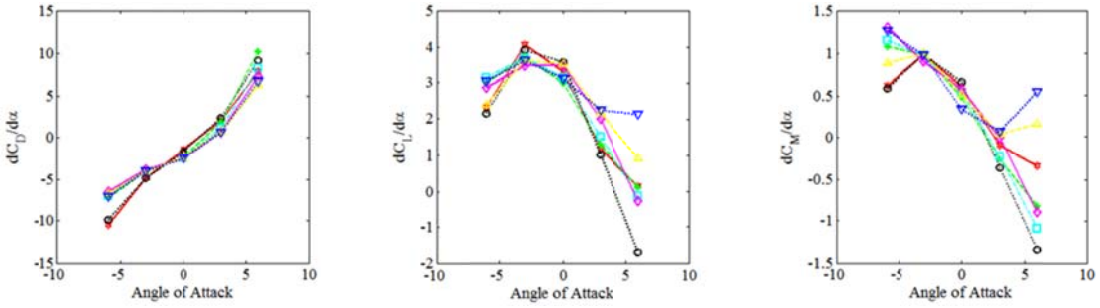

(a) $dC_D/d\alpha$ (b) $dC_L/d\alpha$ (c) $dC_M/d\alpha$

Fig. 12 Derivative of force coefficients with respect to the angle of attack, 1.27×10^6 1.70×10^6 2.60×10^6 3.47×10^6 4.40×10^6 5.24×10^6 6.13×10^6

4.3 Re effects on aerodynamic load sharing between the two girders

Figs. 13 and 14 show the variations of the ratio of the loading on each girder to the total effective force due to the Re. Each aerodynamic force component obtained from pressure measurement was considered as the total effective force on the deck and loading on each girder was estimated by integrating the mean pressures over a single girder. The results show some Re dependence of the load shared by each girder. The drag force was mainly carried by the upstream girder. As shown in Fig. 7, negative pressure was formed on the upper surface of the upstream girder which balanced the negative pressures on the bottom surface, thus reducing the net downward lift. Such pressure equalization was not evident for the downstream girder (as shown in Fig. 7), which resulted in a significant downward lift for the downstream girder which shared most of the total lift.

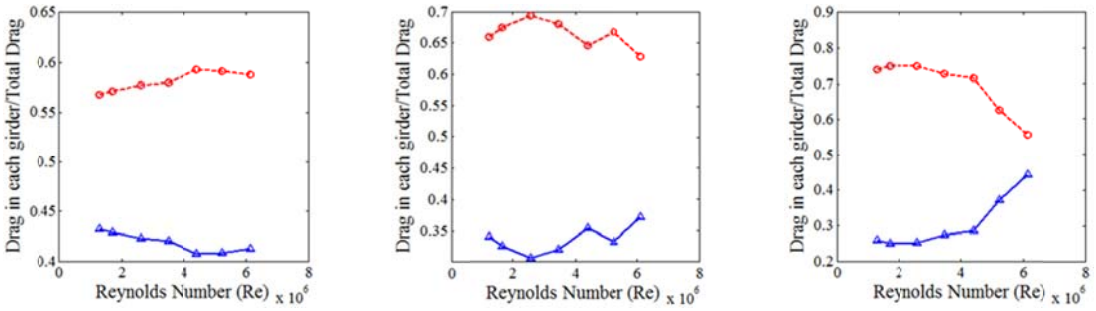

(a) Angle of attack= −3° (b) Angle of attack= 0° (c) Angle of attack= +3°

Fig. 13 Allotment of each girder from drag, Upstream Downstream

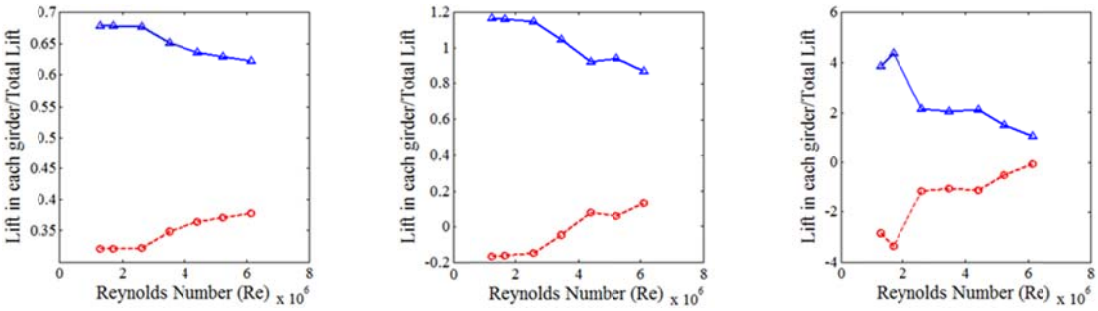

(a) Angle of attack= −3° (b) Angle of attack= 0° (c) Angle of attack= +3°

Fig. 14 Allotment of each girder from lift, Upstream Downstream

Testing at higher Re led to a more even distribution of loads between the two girders, with the exception of drag for -3° wind angle of attack. For this cross section, drag was mainly generated from the pressures on the inclined surfaces of the girders. For the higher Re, similar pressures formed on the inclined surfaces of the two girders. The ratio of the drag taken by each girder to the total drag was quite similar for the two girders which is in agreement with the results on drag presented in Lee *et al.* (2014). Lee *et al.* (2014) expressed that the sheltering effect is minimized with the Re increase, resulting in more uniform load sharing between the two girders.

Fig. 14 shows the ratio of the lift force in each girder to the total lift. Note that the total lift, as shown in Fig. 11, was a negative value (downward force) at all different wind angles of attack for the entire Re range tested. It can be seen that the lift was not distributed equally between the two girders, particularly for the zero and positive wind angles of attack. It can be noticed that the upstream girder was under a positive (upward) lift for the zero and positive wind angles of attack at lower Re. This happened due to the large negative pressures caused by the traffic barrier at the leading edge of the upstream girder (see Figs. 7(c) and 7(d)). However, with the Re increase, pressure distribution changed around the girders and as a result a downward lift was formed on the upstream girder at higher Re.

4.4 Re effects on vortex shedding

Fig. 15 shows the lift coefficient power spectral density against the reduced frequency for the bare deck at the maximum and minimum tested wind speeds and for -6°, 0° and +6° wind angles of attack. Similar plots were obtained to find St for the other wind speeds and wind angles of attack but are not shown for brevity. The sensitivity of the Strouhal number to the Re for the bare deck pitched to different angles is illustrated in Fig. 16.

As shown in Fig. 15, a distinct peak is distinguished in the lift coefficient spectra showing that the bare deck cross section was subjected to vortex shedding. It is also evident that for the larger Re, larger peaks were observed for the zero and +6° wind angles of attack, meaning that vortices shed with higher energy at higher Re. From Fig. 16, it is noticed that St for the bare deck in the negative angles of attack was less Re dependent compared to the zero and positive angles of attack. For the zero and +3° wind angle of attack, St varied inconsistently with the Re increase with an overall decreasing trend. For the +6° wind angles of attack a decreasing trend was noticed.

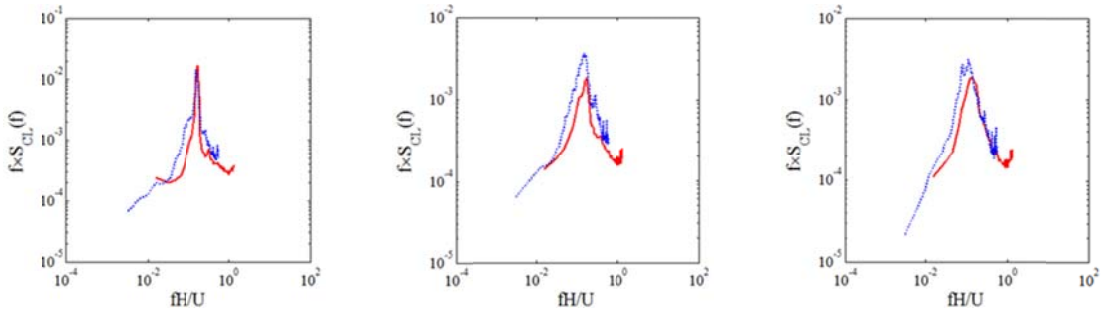

(a) Angle of attack= $-6°$ (b) Angle of attack= $0°$ (c) Angle of attack= $+6°$

Fig. 15 Normalized lift spectra, ——1.27×10^6 ·····6.13×10^6

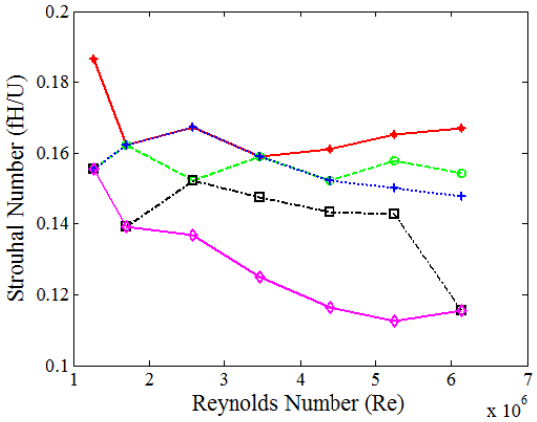

Fig. 16 Strouhal number as a function of Re, —— -6° -·-·- -3° ····· 0° -·-·- +3° —— +6°

Previous literature suggests that three mechanisms may lead to vortex shedding in a twin girder bridge (Kwok *et al.* 2012, Laima *et al.* 2013). The first and second mechanisms are the flow separation over the trailing edges of the upstream and downstream girders, respectively. Third mechanism is the buffeting action of the shed vortices from the upstream girder on the downstream girder. Fig. 17 shows the pressure spectra at the critical locations known as the sources of vortex shedding for the bare deck at 0° angle. It is noticed that the first and third mechanisms were more critical compared to the flow separation from the trailing edge of the downstream girder. The peaks of the pressure spectra were in better agreement with St values calculated from the lift spectra at higher Re (Fig. 17). This means that by increasing the Re, better agreement was observed between the peaks of the pressure spectra and the St values calculated from the lift spectra for all possible mechanisms of vortex shedding.

4.5 Effect of vortex generators

As discussed in Section 4.4, the bare bridge deck cross section was subjected to the vortex shedding. In order to mitigate vortex shedding, diverging pairs of rectangular plates were attached to the bottom flat surface of the two decks. Plates were placed on the upstream side of the gap to keep the approaching wind attached to the surface and guided it to flow into the gap and stopped the formation of vortices by creating a pair of counter rotating helical vortices. The sectional model fitted with the vortex generators is shown in Fig. 18.

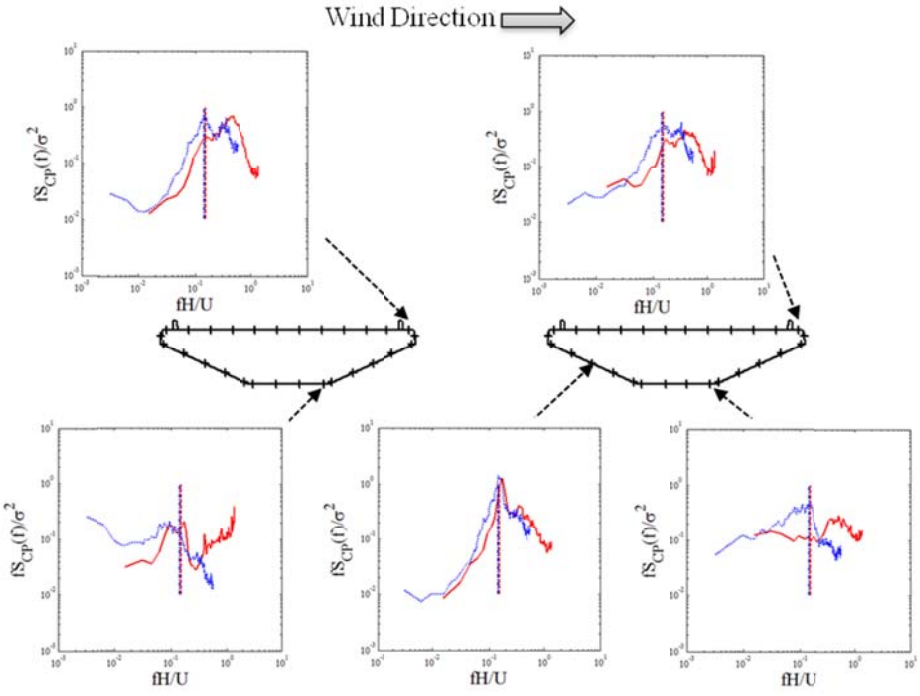

Fig. 17 Pressure spectra at 0° wind angle of attack (Dashed lines show the St found from lift spectra), ——1.27×10^6 ····· 6.13×10^6 — —1.27×10^6 — — 6.13×10^6

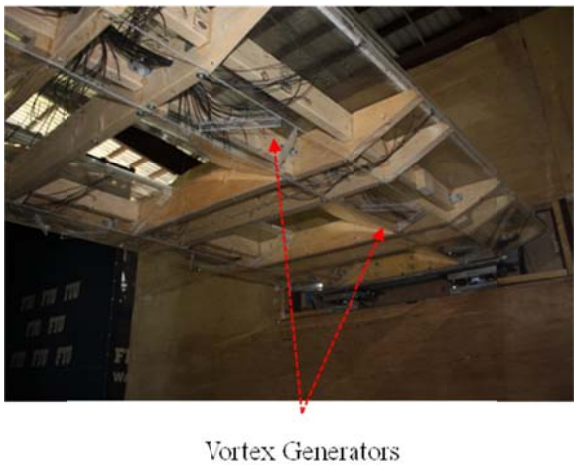

Fig. 18 Vortex generators at bottom surface

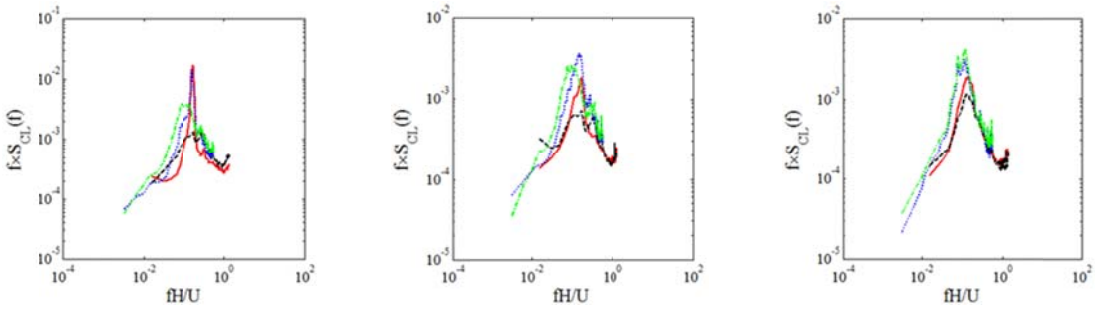

(a) Angle of attack= $-6°$ (b) Angle of attack= $0°$ (c) Angle of attack= $+6°$

Fig. 19 Normalized lift spectra, Bare section: —— 1.27×10^6 ..... 6.13×10^6, Equipped with vortex generators ----- 1.27×10^6 -.-.- 6.13×10^6

Fig. 19 shows the comparison of the lift coefficient power spectral density against the reduced frequency for the deck equipped with the vortex generators and the bare cross section at the maximum and minimum tested wind speeds for -6°, 0°, and +6° angles of wind attack. From Fig. 19, it is evident that adding the vortex generator to the bare section eradicated the apparent spectral peak in the lift spectrum. It seems that the mitigation devices were more effective in the low Re regime, particularly for the zero and negative wind angles of attack. With the Re increase a new peak formed in the lift coefficient spectrum at a smaller reduced frequency compared to the original section St. Unlike the bare section, this peak in the spectrum was distributed over a wider range of frequencies and was weaker. It is hypothesized that by increasing the Re, the two counter rotating vortices got mixed and flow separated from the surface. Therefore, a new wake region formed from vortices that were shed at a broad range of frequencies.

5. Conclusions

In order to evaluate Re effects on aerodynamic characteristics of a twin-deck bridge, a sectional model was tested in a uniform flow. The pressure distribution and aerodynamic forces were measured over a Re range from 1.3×10^6 to 6.1×10^6 based on the deck width. The variation in the turbulence intensities was not significant and for the larger wind speeds it was almost a constant value around 3.0 percent. The following experimental observations were made:

1. The studied bridge section showed different behavior with regards to the Re dependency for different angles of attack, showing higher dependency on *Re* for positive angles of attack.
2. Flow separated from the top surface of the upstream girder at the location of the upwind traffic barrier. For negative angles of attack the separation and reattachment points were almost fixed and the flow pattern changes due to the Re were negligible.
3. At zero and +3° wind angles of attack, the structure of flow within the gap region changed by the Re increase. Pressure distribution on the windward inclined surface of the downstream girder and on the leeward tipping edge of the upstream girder changed noticeably with Re.
4. For the zero wind angle of attack which is the most important wind direction, the maximum drag coefficient change was noticed to be around 8% while lift coefficient changed more than 70%, for the change in Re values simulated.
5. The derivative of the aerodynamic force coefficients with respect to the wind angle of attack changed with Re for the case of positive angles of attack. The results suggest that testing at lower Re regime is conservative for aeroelastic analysis of flutter.
6. For zero and positive wind angles of attack with increases in Re, the distribution of the pressures around the upstream girder moved closer to the pressure distribution around the downstream girder. This means that Re increase helped in sharing loads more uniformly between the two girders.
7. Vortex shedding of this twin-deck bridge was mainly governed by the vortex shedding from the trailing edge of the upstream deck and its impingement on the downstream deck. Adding a pair of diverging vortex generators to the bottom surface of the girders was effective in mitigating the vortex shedding, particularly at lower Re values.

Acknowledgements

This research was supported by the National Science Foundation (NSF) [NSF MRI Award CMMI-0923365] and Florida Center of Excellence in Hurricane Damage Mitigation and Product Development for acquisition of instruments. The authors also would like to acknowledge Maryam Asghari Mooneghi, Walter Conklin and Roy Liu Marques of Wall of Wind, FIU for their unreserved input during testing. The findings reported in this article are those of the authors alone, and do not necessarily represent the views of sponsoring agencies. We also acknowledge the contribution of T.Y. Lin International in providing us with information on the East Bay Bridge. The results provided in the paper do not extrapolate directly to the East Bay Bridge as the geometry was simplified for the purposes of the present research.

References

Asghari Mooneghi, M., Irwin, P. and Gan Chowdhury, A. (2014), "Large-scale testing on wind uplift of roof pavers", *J. Wind Eng. Ind. Aerod*., **128**, 22-36.

Barre, C. and Barnaud, G. (1993), "High Reynolds number simulation techniques and their application to shaped structures model test", *Proceedings of the 1st IAWE European and African Regional Conference on Wind Engineering*, Guernsey UK.

Chen, X. and Kareem, A. (2002), "Advances in modeling of aerodynamic forces on bridge decks", *J. Eng. Mech. - ASCE*, **128**(11), 1193-1205.

Chowdhury, A.G. and Sarkar, P.P. (2004), "Identification of eighteen flutter derivatives of an airfoil and a bridge deck", *Wind Struct*., **7**(3), 187-202.

Gu, M., Zhang, R. and Xiang, H. (2001), "Parametric study on flutter derivatives of bridge decks", *Eng. Struct*., **23**(12), 1607-1613.

Irwin, P., Cooper, K. and Girard, R. (1979), "Correction of distortion effects caused by tubing systems in measurements of fluctuating pressures", *J. Wind Eng. Ind. Aerod*., **5**(1-2), 93-107.

Kazutoshi, M., Masafumi, T. and Tooru, I. (2007), "Reynolds number effects on the steady and unsteady aerodynamic forces acting on the bridge deck sections of long-span suspension bridge", *IHI Eng. Rev*., **40**(1), 12-26.

Kubo, Y., Nogami, C., Yamaguchi, E., Kato, K., Niihara, Y. and Hayashida, K. (1999). "Study on Reynolds number effect of a cable-stayed bridge girder, (Eds., A. Larsen, G.L. Larose and F.M. Livesey)", *Proceedings of the Wind Engineering into the 21st Century*, Balkema, Rotterdam.

Kwok, K.C.S., Qin, X.R., Fok, C.H. and Hitchcock, P.A. (2012), "Wind-induced pressures around a sectional twin-deck bridge model: Effects of gap-width on the aerodynamic forces and vortex shedding mechanisms", *J. Wind Eng. Ind. Aerod*., **110**, 50-61.

Laima, S., Li, H., Chen, W. and Li, F. (2013), "Investigation and control of vortex-induced vibration of twin box girders", *J. Fluid. Struct*., **39**, 205-221.

Larose, G.L. and D'Auteuil, A. (2006), "On the Reynolds number sensitivity of the aerodynamics of bluff bodies with sharp edges", *J. Wind Eng. Ind. Aerod*., **94**(5), 365-376.

Larose, G.L., Larsen, S.V., Larsen, A., Hui, M. and Jensen, A.G. (2003), "Sectional model experience at high Reynolds number for the deck of a 1 018 m span cable-stayed br idge", *Proceedings of the 11th International Conference on Wind Engineering*, Lubbock Texas USA.

Larose, G.L. and Livesey, F.M. (1997), "Performance of streamlined bridge decks in relation to the aerodynamics of a flat plate", *J. Wind Eng. Ind. Aerod*., **69-71**, 851-860.

Larose, G.L., Wall, A., McAuliffe, B.R., Kelly, D., Stone, G. and Yakymyk, W. (2012), "Sectional model investigation at high Reynolds number for a super tall building", *J. Wind Eng. Ind. Aerod*., **104-106**, 49-55.

Larsen, A., Savage, M., Lafrenière, A., Hui, M.C.H. and Larsen, S.V. (2008), "Investigation of vortex response of a twin box bridge section at high and low Reynolds numbers", *J. Wind Eng. Ind. Aerod*., **96**(6-7), 934-944.

Lee, S., Kwon, S.D. and Yoon, J. (2014), "Reynolds number sensitivity to aerodynamic forces of twin box bridge girder", *J. Wind Eng. Ind. Aerod*., **127**, 59-68.

Matsuda, K., Cooper, K.R., Tanaka, H., Tokushige, M. and Iwasaki, T. (2001), "An investigation of Reynolds number effects on the steady and unsteady aerodynamic forces on a 1:10 scale bridge deck section model", *J. Wind Eng. Ind. Aerod*., **89**(7-8), 619-632.

Neuhaus, C. and Höffer, R. (2011), "Identification of quasi-stationary aeroelastic force coefficients for bridge deck sections using forced vibration wind tunnel testing", *Proceedings of the 8th International Conference on Structural Dynamics*, EURODYN 2011, Leuven, Belgium.

Piña, R.B. and Caracoglia, L. (2009), "Extraction of flutter derivatives from small-scale wind tunnel experiments", *Proceedings of the 11th Americas Cnference on Wind Engineering*, San Juan, Puerto Rico.

Scanlan, R.H. (1978), "The action of flexible bridges under wind, I: Flutter theory", *J. Sound Vib*., **60**(2), 187-199.

Schewe, G. (2001), "Reynolds number effects in flow around a more-or-less bluff bodies", *J. Wind Eng. Ind.*

Aerod., **89**(14-15), 1267-1289.
Schewe, G. (2009), "Reynolds-number-effects in flow around a rectangular cylinder with aspect ratio 1:5", *Proceedings of the 5th European & African Conferences on Wind Engineering (EACWE 5) Florence*, Italy, 19th-23rd July.
Schewe, G. and Larsen, A. (1998), "Reynolds number effects in the flow around a bluff bridge deck cross section", *J. Wind Eng. Ind. Aerod*., **74-76**, 829-838.
Wardlaw, R.L., Tanaka, H. and Utsunomiya, H. (1983), "Wind tunnel experiments on the effects of turbulence on the aerodynamic behaviour of bridge road decks", *J. Wind Eng. Ind. Aerod*., **14**(1-3), 247-257.
Wu, T. and Kareem, A. (2012), "An overview of vortex-induced vibration (VIV) of bridge decks", *Frontiers Struct. Civil Eng*., **6**(4), 335-347.